# Experimental $g$ factor and $B(E2)$ value of the $4_1^+$ state in Coulomb-excited $^{66}$Zn compared to shell-model predictions

J. Leske, K.-H. Speidel, and S. Schielke
*Helmholtz-Institut für Strahlen- und Kernphysik, Universität Bonn, Nussallee 14-16, D-53115 Bonn, Germany*

J. Gerber
*Institut de Recherches Subatomiques, F-67037 Strasbourg, France*

P. Maier-Komor
*Physik-Department, Technische Universität München, James-Franck-Straße, D-85748 Garching, Germany*

T. Engeland and M. Hjorth-Jensen
*Department of Physics and Center of Mathematics for Applications, University of Oslo, N-0316 Oslo, Norway*
(Received 15 March 2006; published 20 June 2006)

The $g$ factor of the $4_1^+$ state in $^{66}$Zn has been measured for the first time employing the technique of projectile Coulomb excitation in inverse kinematics combined with transient magnetic fields. The lifetime of this state, $\tau(4_1^+) = 1.1(2)$ ps, which has been remeasured by the Doppler shift attenuation method, is twice as large as a previously determined value. Both the deduced $B(E2; 4_1^+ \rightarrow 2_1^+) = 133(24)\ e^2\ \mathrm{fm}^4$ and the $g$ factor of the $4_1^+$ state, $g(4_1^+) = +0.65(20)$, were interpreted, together with results for the $2_1^+$ state, in the framework of shell-model calculations based on a $^{56}$Ni closed-shell core. The present results are also compared with those for neighboring $^{64}$Zn and $^{68}$Zn that were obtained in previous measurements by the same technique.

DOI: 10.1103/PhysRevC.73.064305 PACS number(s): 21.10.Tg, 21.10.Ky, 25.70.De, 27.50.+e

## I. INTRODUCTION

The low-level structure of stable even-$A$ Zn isotopes has been systematically investigated in several recent experiments by comparing $g$-factor data and $B(E2)$ values, with emphasis on the $2_1^+$ states and to a lesser extent on $4_1^+$ states, with results from shell-model calculations based on highly developed shell-model codes [1–3]. In the measurements, the combined technique of projectile Coulomb excitation in inverse kinematics and transient magnetic fields (TF) has been effectively employed to excite the Zn projectiles by scattering from a carbon target; ferromagnetic gadolinium provided the intense TF for the spin precessions of the nuclei in their short-lived excited states. The $B(E2)$ values were deduced from newly determined nuclear lifetimes for which the Doppler shift attenuation method (DSAM) was utilized. On the theoretical side, the shell-model calculations were based on the full $fp$-shell configuration space assuming either $^{40}$Ca or $^{56}$Ni as inert cores and the most commonly used effective $NN$ interactions of $fp$-shell nuclei [4,5]. In comparison with the experimental data, good agreement was generally found. However, there are also significant deviations, which have been attributed to restrictions in the model space and also to omitted degrees of freedom in terms of meson-exchange currents and particle-hole excitations of the respective core nuclei. The latter aspect has been particularly discussed and emphasized in a recent article on $^{68}$Zn [3].

Specifically, for $^{68}$Zn, the $g$ factor of the $4_1^+$ state was found to be negative, $g(4_1^+) = -0.37(17)$, a most surprising result [3], in view of the positive value, $g(4_1^+) = +0.53(16)$, measured for $^{64}$Zn, particularly because all the above-mentioned shell-model calculations clearly predict a positive $g$ factor for $^{68}$Zn as well (see, e.g., Ref. [1]). This unexpected observation required new theoretical considerations in which the neutron $0g_{9/2}$ orbital is likely to play a more dominant role in the $4_1^+$ wave function, bearing in mind that the Schmidt value is $g(\nu g_{9/2}) = -0.425$. Indeed, the newly calculated value for $^{68}$Zn, $g(4_1^+) = +0.008$, turned out to be very small and significantly lower in absolute magnitude than that predicted for $^{64}$Zn, but the negative sign of the experimental value could not be verified. In this context it was further argued that an inert $^{56}$Ni core (as used in the calculations) prohibited additional negative contributions to the $g$ factor because of the coupling of $0f_{7/2}$ neutron-hole configurations with the $1p_{3/2}$ orbital (see also Ref. [3]).

In view of these fundamentally new insights into the structure of Zn nuclei in general, additional $g$ factor measurements were performed on the neighboring isotope $^{66}$Zn, to search for a transitional behavior from the large positive $g(4_1^+)$ value of $^{64}$Zn to the negative value for $^{68}$Zn. Simultaneously, the lifetime and the deduced $B(E2)$ of the $(4_1^+ \rightarrow 2_1^+)$ transition have been redetermined to check the validity of the observed large $B(E2)$ value [6], which significantly exceeded the corresponding values for both neighboring isotopes $^{64}$Zn and $^{68}$Zn, as well as shell-model predictions. In addition to these data more information has been obtained for the $2_1^+$ and the $3_1^-$ states that can be compared with corresponding results on $^{64}$Zn and $^{68}$Zn.

## II. EXPERIMENTAL DETAILS

For the current measurements a beam of isotopically pure $^{66}$Zn, provided as $ZnO^-$ ions by the ion source, was accelerated to 180 MeV at the Munich tandem accelerator,

 

thereby exposing the multilayered target to beam intensities of $\sim$25 *e*nA. The target consisted of 0.44 mg/cm$^2$ natural carbon deposited on a 3.34 mg/cm$^2$ Gd layer, which was evaporated on a 1.4 mg/cm$^2$ Ta foil backed by a 4.49 mg/cm$^2$ Cu layer. Thin layers of natural titanium of $\sim$0.005 mg/cm$^2$ thickness were placed between C and Gd and between Ta and Cu to ensure good adherence of these layers. This preparation technique was also found to be very successful in other experiments involving heavy-ion beams. In the measurements, the target was cooled to liquid nitrogen temperature and magnetized to saturation in an external field of 0.06 Tesla.

The $^{66}$Zn projectiles were Coulomb excited by scattering from the carbon layer, the carbon recoils being detected in a 100 $\mu$m Si detector located at 0° relative to the beam axis. For this purpose a Ta beam stopper was placed between target and detector which, however, permitted the carbon ions to pass through to the detector. The excited Zn nuclei resulting from the collisions with the carbon nuclei moved with a mean velocity of $\sim$5.8 $v_0$ ($v_0 = e^2/\hbar$) through the Gd layer, experiencing spin precessions in the TF, and were ultimately stopped in the hyperfine-interaction-free environment of the Cu backing. In addition to Coulomb excitation of $^{66}$Zn, excited states of the $^{70}$Ge isotope were populated in the $\alpha$-transfer reaction. In this case, the two $\alpha$ particles from the decay of the formed $^{8}$Be nuclei were well separated in pulse-height from the carbon ions in the particle spectrum of the Si detector. Hence, coincident $\gamma$ rays of transitions in $^{70}$Ge were well distinguished from those of $^{66}$Zn and no conflicting overlap of the two nuclei was observed. The results for $^{70}$Ge will be reported in a separate forthcoming publication [7].

The deexcitation $\gamma$ rays of $^{66}$Zn were measured in coincidence with the forward-scattered carbon ions, giving rise to exceptionally clean spectra that permitted determining photopeak intensities with high reliability. The relevant level scheme of $^{66}$Zn is shown in Fig. 1. For $\gamma$ detection 12.7 cm × 12.7 cm

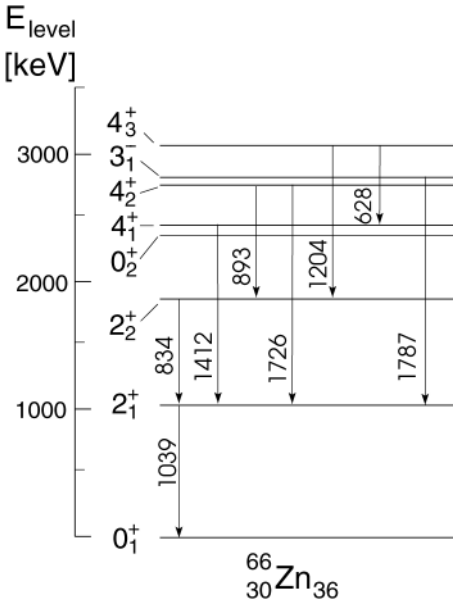


FIG. 1. Low-lying states and $\gamma$ transitions of $^{66}$Zn relevant to the present measurements.

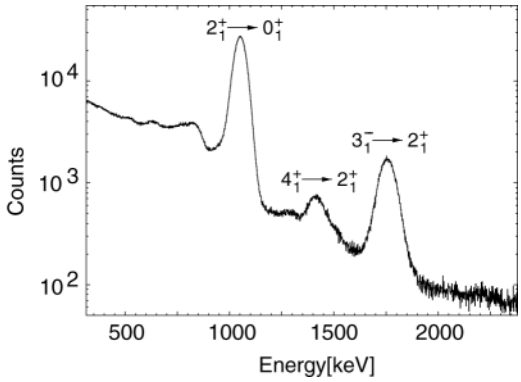


FIG. 2. $\gamma$-coincidence spectrum for $^{66}$Zn observed with a large-volume NaI(Tl) scintillator located at $\Theta_\gamma = 65°$. The assigned transitions refer to the present investigations (see text).

NaI(Tl) scintillators were used whose energy resolution was sufficient for safe distinction of the transitions of interest (see Fig. 2). In addition, a Ge detector with 40% relative efficiency was placed at 0°, serving as a monitor for contaminant $\gamma$ lines and for measuring the lifetimes of the states in question. Figure 3 shows a typical coincidence spectrum of the Ge detector in which all $\gamma$ lines are well resolved and surely attributed solely to Coulomb excited $^{66}$Zn. The Doppler-broadened lines reflect the nuclear lifetimes.

Particle-$\gamma$ angular correlations $W(\Theta_\gamma)$ have been measured for determining the logarithmic slopes, $|S| = [1/\mathrm{W}(\Theta_\gamma)]\cdot[\mathrm{dW}(\Theta_\gamma)/\mathrm{d}\Theta_\gamma]$, in the rest frame of the $\gamma$-emitting nuclei at $\Theta_\gamma^{\mathrm{lab}} = \pm 65°$ and $\pm 115°$, where the sensitivity to the spin precessions was optimal for all the transitions in question. Precession angles, $\Phi^{\mathrm{exp}}$, were derived from counting-rate ratios $R$ for up and down directions of the external magnetizing field that can be expressed as [1,2],

$$\Phi^{\mathrm{exp}} = \frac{1}{S}\cdot\frac{\sqrt{R}-1}{\sqrt{R}+1} = g\frac{\mu_N}{\hbar}\int_{t_{\mathrm{in}}}^{t_{\mathrm{out}}} B_{\mathrm{TF}}[v_{\mathrm{ion}}(t)]e^{-\frac{t}{\tau}}dt, \quad (1)$$

where $g$ is the $g$ factor of the nuclear state and $B_{\mathrm{TF}}$ is the TF acting on the nucleus during the time interval $(t_{\mathrm{out}} - t_{\mathrm{in}})$

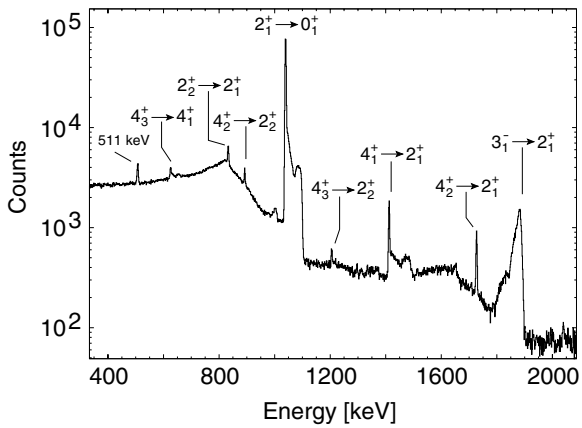


FIG. 3. The same coincidence spectrum as shown in Fig. 2 by using a Ge detector located at $\Theta_\gamma = 0°$. Most of the assigned lines are identified according to the level scheme shown in Fig. 1. The Doppler-broadened line shapes reflect the nuclear lifetimes.

TABLE I. Summary of the experimental logarithmic slopes of the angular correlations at $\Theta_\gamma^{\rm lab} = 65^\circ$, the precession angles and lifetimes of the states in question for $^{66}$Zn. The $\Phi^{\rm lin}/g$ values were calculated using Eqs. (1)–(3). The deduced $g$ factors and the newly measured lifetimes are compared with literature values (see Ref. [1] and references therein).

| $E_x(I^\pi)$ (MeV) | $I^\pi$ | $\tau$ (ps) | | $\lvert S(\Theta_\gamma)\rvert$ (mrad)$^{-1}$ | $\Phi^{\rm exp}$ (mrad) | $\Phi^{\rm lin}/g$ (mrad) | $g(I)$ | |
|---|---|---|---|---|---|---|---|---|
| | | Present | [1,6,11] | | | | Present | [1] |
| 1.039 | $2_1^+$ | 2.5(1) | 2.43(4) | 1.904(7) | 14.0(2) | 26.5(2.6) | +0.53(5) | +0.40(4) |
| 2.451 | $4_1^+$ | 1.1(2) | 0.52(2) | 0.79(8) | 15.2(4.5) | 23.5(2.4) | +0.65(20) | — |
| 2.826 | $3_1^-$ | 0.26(1) | 0.26(4) | 0.23(2) | 9.2(4.3) | 13.1(1.3) | +0.7(3) | — |
| 3.077 | $4_3^+$ | 1.5(1) | — | — | — | — | — | — |

that the ions spend in the gadolinium layer of the target; the exponential accounts for nuclear decay with lifetime $\tau$ in the Gd layer.

The nuclear lifetimes have been measured simultaneously with the precessions using the DSAM technique. For the analysis of the Doppler-broadened line shapes the computer code LINESHAPE [8] has been used. Details of the analysis procedure and the stopping powers [9] used are reported in Ref. [10].

## III. RESULTS AND DISCUSSION

The $g$ factors were derived from the experimental precession angles by determining the effective transient field $B_{\rm TF}$ on the basis of the empirical linear parametrization (see, e.g., Ref. [10]):

$$B_{\rm TF}(v_{\rm ion}) = G_{\rm beam} \cdot B_{\rm lin}, \tag{2}$$

with

$$B_{\rm lin} = a(Gd) \cdot Z_{\rm ion} \cdot v_{\rm ion}/v_0, \tag{3}$$

where $a$(Gd) = 17(1) T and $G_{\rm beam} = 0.61(6)$ is the empirical attenuation factor accounting for the demagnetization of the Gd layer induced by the energetic Zn beam. Its magnitude has been determined from a large body of experimental data for the present actual conditions in terms of the energy loss of the beam ions and the mean velocity of the excited Zn ions in the Gd layer (see also Refs. [2,10]).

The observed precessions and lifetimes are summarized in Table I. The deduced $g$ factors and the newly determined lifetimes have been compared with previous results quoted in the literature. For all states in question the lifetimes are well reproduced, with the sole exception of that of the $4_1^+$ state. For the latter, our result is twice as large as the value recently obtained by Koizumi *et al*. [6]. It is interesting to note that their value of $\tau = 0.52(2)$ ps was already significantly larger than that of the previously known value in the literature, $\tau = 0.26(6)$ ps [11]. It should further be noted that in our lifetime analyses an average 10% correction because of feeding transitions has been included (see also Fig. 3). Because of the striking discrepancy in the lifetime for the $4_1^+$ state between literature and the present result this correction was under particularly close scrutiny. Line-shape fits of the $(2_1^+ \rightarrow 0_1^+)$, $(4_1^+ \rightarrow 2_1^+)$, and the $(3_1^- \rightarrow 2_1^+)$ transitions are shown in Fig. 4. Respective feeding fractions contributing to the stopped components and the individual background level included in the fit are also displayed. The lifetime of the $4_3^+$ state at 3.077 MeV has been determined for the first time.

The $g$ factor of the $2_1^+$ state turned out to be slightly larger than the previous value, whereby the quoted error in both values is mainly determined by that of the attenuation factor $G_{\rm beam}$ of the TF. The origin of this marginal discrepancy might be related to small differences in the Gd magnetization of the two different targets used that had been assumed to be equal.

As is evident from Table I the $g$ factor of the $4_1^+$ state in $^{66}$Zn is definitely positive and of the same magnitude

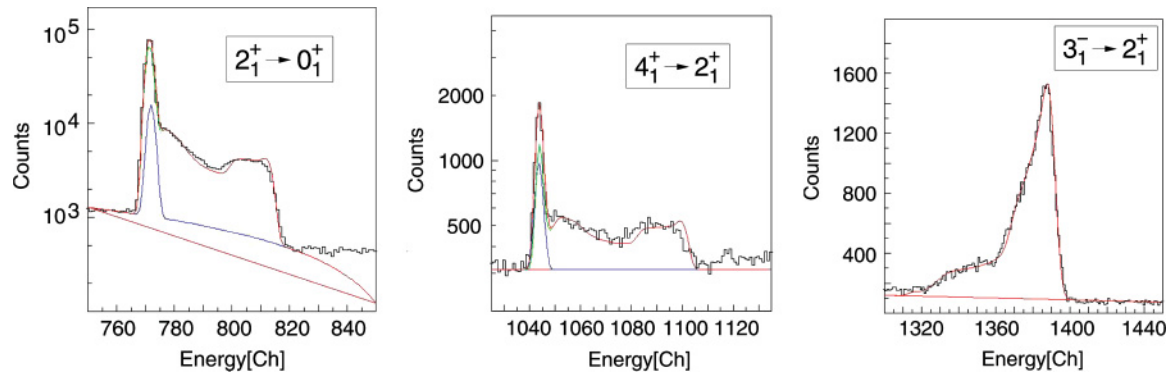


FIG. 4. (Color online) DSAM fits to the Doppler-broadened shapes of three $\gamma$ lines in $^{66}$Zn. The individual experimental contributions of feeding from higher states to the stopped components are also displayed.

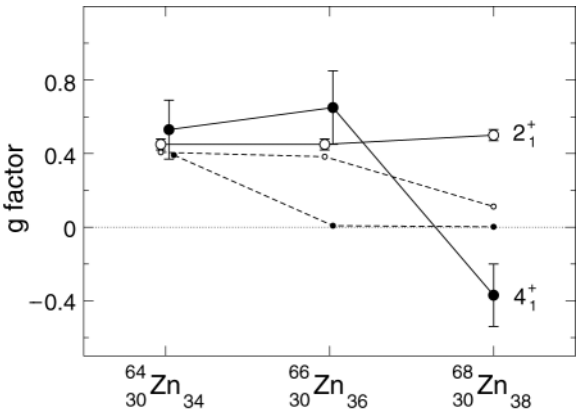


FIG. 5. Experimental $g$ factors of the $2_1^+$ and $4_1^+$ states in $^{66}$Zn in comparison to corresponding results for the neighboring isotopes $^{64}$Zn and $^{68}$Zn [3]. Results from large-scale shell-model calculations (SM-3) are also displayed (small symbols). The lines drawn are to guide the eye (see text).

as that in $^{64}$Zn but in clear contrast to the negative value observed for the corresponding $4_1^+$ state in $^{68}$Zn. This dramatic variation with neutron number, however, is not seen in the $g(2_1^+)$ values of these isotopes, which are roughly constant or imply a very weakly rising tendency with increasing neutron number. The strikingly different behavior of the $g$ factors for the $2_1^+$ and $4_1^+$ states of these three isotopes is demonstrated in Fig. 5.

The $B(E2)$ value of the $(4_1^+ \rightarrow 2_1^+)$ transition of 133(24) $e^2$ fm$^4$ in $^{66}$Zn, deduced from the present lifetime of the $4_1^+$ state, is distinctly smaller than that of Ref. [6] of 278(11) $e^2$ fm$^4$ but is consistent with the trend indicated by the data for the neighboring $^{64}$Zn and $^{68}$Zn isotopes, of 185(7) and 166(9) $e^2$ fm$^4$, respectively [3]. This new result is also shown in Fig. 6.

In the following we have attempted to understand these results in the framework of large-scale shell-model calculations based on the same model space and the effective interaction discussed in great detail in our recent article with emphasis on the surprising $g$ factor result for the $4_1^+$ state in $^{68}$Zn [3]. In these considerations it was shown, as mentioned, that the neutron $0g_{9/2}$ configuration is the dominant component in the nuclear wave function implying a negative $g$ factor as also observed for low-lying $9/2^+$ states in neigboring odd-$A$ Zn isotopes [12]. The calculations yielded in this case a vanishingly small $g(4_1^+)$ value, in contrast to the distinctly positive value of its even-$A$ $^{64}$Zn neighbor, but were not able to verify the negative sign of the measured value. In this work we have extended these calculations to $^{66}$Zn. We repeat here some of the calculational details of Refs. [2,3]. To study the importance of the $0g_{9/2}$ orbit we have performed shell-model calculations using $^{56}$Ni as closed-shell core, with a model space defined by protons and neutrons occupying the single-particle orbitals $0f_{5/2}$, $1p_{3/2}$, $1p_{1/2}$, and $0g_{9/2}$ ($0f_{5/2}1pg_{9/2}$). To determine the effective interaction we use the recent charge-dependent potential model of Machleidt, the so-called CD-Bonn interaction [13]. The final effective two-body interaction is obtained via many-body perturbation theory to third order, employing a renormalized nucleon-nucleon interaction defined for $^{56}$Ni as closed-shell core and including folded diagrams to infinite order. For details, see, for example, Ref. [14]. A harmonic oscillator basis was used, with an oscillator energy determined via $\hbar\Omega = 45A^{-1/3} - 25A^{-2/3} = 10.1$ MeV, $A = 56$ being the mass number. For the single-particle energies we employ values adapted from Grawe in Ref. [15], resulting in the energy differences $\epsilon_{0g_{9/2}} - \epsilon_{1p_{3/2}} = 3.70$ MeV, and $\epsilon_{0f_{5/2}} - \epsilon_{1p_{3/2}} = 0.77$ MeV, and $\epsilon_{1p_{1/2}} - \epsilon_{1p_{3/2}} = 1.11$ MeV for neutrons and $\epsilon_{0g_{9/2}} - \epsilon_{1p_{3/2}} = 3.51$ MeV, $\epsilon_{0f_{5/2}} - \epsilon_{1p_{3/2}} = 1.03$ MeV, $\epsilon_{1p_{1/2}} - \epsilon_{1p_{3/2}} = 1.11$ MeV for protons. The effective interaction has not been corrected for any possible monopole changes. This means that the only parameters that enter our calculations are those defining the nucleon-nucleon interaction fitted to reproduce the scattering data, the experimental single-particle energies and the oscillator basis. We have also carried out calculations with a different value for the neutron $0g_{9/2}$ energy, namely $\epsilon_{0g_{9/2}} - \epsilon_{1p_{3/2}} = 4.00$ MeV. Furthermore, for the computation of the $B(E2)$'s and $g$ factors, we have used unrenormalized magnetic moments and the canonical unrenormalized charges for protons and neutrons. The latter entails charges of 1.5 $e$ and 0.5 $e$ for protons and neutrons, respectively. The free nucleon operator for the magnetic moment is defined as

$$\mu_{\text{free}} = g_l l + g_s \mathbf{s}, \tag{4}$$

with $g_l(\text{proton}) = 1.0$, $g_l(\text{neutron}) = 0.0$, $g_s(\text{proton}) = 5.586$, $g_s(\text{neutron}) = -3.826$.

In Table II we display the results from the two above-mentioned sets of calculations, SM-3 and SM-4, for $^{66}$Zn. The first line shows the results obtained with the single-particle

TABLE II. Comparison of experimental excitation energies, average $g$ factors and $B(E2)$ values (deduced from lifetimes, see Table I) of $^{66}$Zn with results from present shell-model calculations SM-3 and SM-4 (see text for further details).

| $E(I_f^\pi)$ (MeV) | | $I_f^\pi \rightarrow I_i^\pi$ | $\langle\tau(I_f^\pi)\rangle$ (ps) | $g(I_f^\pi)$ | | $B(E2)\downarrow$ [$e^2$ fm$^4$] | |
|---|---|---|---|---|---|---|---|
| Exp. | Calc. | | | Exp. | Calc. | Exp. | Calc. |
| 1.039 | 1.102[a] | $2_1^+ \rightarrow 0_1^+$ | 2.44(4) | +0.45(3) | +0.383[a] | 276(5) | 180.5[a] |
| | 1.143[b] | | | | +0.181[b] | | 179.7[b] |
| 2.451 | 2.617[a] | $4_1^+ \rightarrow 2_1^+$ | 1.1(2) | +0.65(20) | +0.008[a] | 133(24) | 190.7[a] |
| | 2.843[b] | | | | +0.112[b] | | 185.4[b] |

[a]SM-3.
[b]SM-4.

TABLE III. Experimental $B(E2)$ values in units of [$e^2$ fm$^4$] and [W.u.] (Weisskopf units) in comparison to shell-model calculations SM-1 ($^{40}$Ca) and SM-2 ($^{56}$Ni, $g_{9/2}$) [1] and SM-3 and SM-4 ($^{56}$Ni, $g_{9/2}$, see text for further details.)

| $^A$Zn Isotope | Unit | $B(E2; 2_1^+ \to 0_1^+)$ | | | | | $B(E2; 4_1^+ \to 2_1^+)$ | | | | |
|---|---|---|---|---|---|---|---|---|---|---|---|
| | | Exp. | SM-1 | SM-2 | SM-3 | SM-4 | Exp. | SM-1 | SM-2 | SM-3 | SM-4 |
| $^{64}$Zn | [$e^2$ fm$^4$] | 307(7) | 234 | 172 | 170.4 | 174.8 | 185(7) | 232.0 | 218.0 | 196.1 | 211.6 |
| | [W.u.] | 20.1(5) | 15.4 | 11.3 | 11.2 | 11.5 | 12.2(5) | 15.3 | 14.3 | 12.9 | 13.9 |
| $^{66}$Zn | [$e^2$ fm$^4$] | 276(5) | 199 | 166.5 | 180.5 | 179.7 | 133(24) | 220.0 | 204.7 | 190.7 | 185.4 |
| | [W.u.] | 17.4(3) | 12.5 | 10.5 | 11.4 | 11.3 | 8.4(15) | 13.8 | 12.9 | 12.0 | 11.7 |
| $^{68}$Zn | [$e^2$ fm$^4$] | 242(3) | 149 | 159.8 | 190.9 | 190.4 | 166(9) | 54 | 179.0 | 224.6 | 236.2 |
| | [W.u.] | 14.7(2) | 9.0 | 9.7 | 11.6 | 11.5 | 10.1(5) | 3.3 | 10.9 | 13.6 | 14.3 |

energy spacing for $\epsilon_{0g_{9/2}} - \epsilon_{1p_{3/2}} = 3.70$ MeV, whereas the second line lists the results obtained with $\epsilon_{0g_{9/2}} - \epsilon_{1p_{3/2}} = 4.00$ MeV. Both sets of calculations yield $B(E2)$ results in fair agreement with experiment and the trends seen in Table III for the other Zn isotopes (see also Fig. 6). Furthermore, the $B(E2)$ values reported here also agree fairly well with previous calculations [1] with fitted interactions, namely the results with a $^{40}$Ca closed-shell core and the $0f1p$-shell (SM-1) and a $^{56}$Ni closed-shell core with the $g_{9/2}$ orbit included (SM-2). These sets of calculations for the $B(E2)$ values of several nuclei do not display large deviations among themselves.

The situation is, however, different when we consider the $g$ factors. Our two calculations (SM-3 and SM-4) reported in Table II exhibit large differences when we vary the $\epsilon_{0g_{9/2}} - \epsilon_{1p_{3/2}}$ neutron energy spacing from 3.70 to 4.00 MeV. It should be noted that the SM-4 calculation yields a more accurate spectroscopic description for the odd Zn nuclei $^{65}$Zn and $^{67}$Zn. The $g(4_1^+)$ factor also exhibits improved agreement with data when we increase the single-particle energy spacing for the $0g_{9/2}$ orbit. However, the agreement for the $g(2_1^+)$ factor becomes poorer. This clearly indicates a strong sensitivity to the $0g_{9/2}$ neutron component in the nuclear wave functions.

If one studies the trend for the $g$ factors for $^{64}$Zn, $^{66}$Zn, and $^{68}$Zn, the experimental values for $g(2_1^+)$ are $+0.45(3)$, $+0.45(3)$, and $+0.50(3)$, respectively. If we employ the SM-3 calculations the corresponding numbers are $+0.407$, $+0.383$, and $+0.112$, respectively (see Fig. 5 and Table IV; note a misprint in Table II of Ref. [3], where the theoretical values for the $g$ factors in the column SM-2 should be divided by their respective spin values). Similarly, with SM-4 we obtain $+0.404$, $+0.181$, and $+0.148$, respectively (see Table IV).

These $g$-factor results should in turn be compared with the SM-1 and SM-2 results of Ref. [1]. The truncated calculations with $^{40}$Ca as closed-shell core yield for the $2_1^+$ states of $^{64}$Zn, $^{66}$Zn, and $^{68}$Zn $+0.48$, $+0.48$, and $+0.58$, whereas the $^{56}$Ni closed-shell core with the $0g_{9/2}$ orbit included gave $+0.448$, $+0.578$, and $+0.733$, respectively. The results of these calculations exhibit in general a much better overall agreement with data than the new calculations reported here. However, for the $g(4_1^+)$, both the SM-1 and SM-2 calculations neither yield the experimental value of $^{68}$Zn nor reproduce its neutron number dependence. The experimental $g(4_1^+)$ factors of $^{64}$Zn, $^{66}$Zn, and $^{68}$Zn are $+0.53(16)$, $+0.65(20)$, and $-0.37(17)$, whereas the corresponding SM-1 and SM-2 results from Ref. [1] are $+0.730$, $+0.740$, and $+1.08$ for SM-1 and $+0.362$, $+0.436$, and $+0.404$ for SM-2, respectively (see also Table IV).

In contrast, our new calculations yield for the $g(4_1^+)$ factor of $^{64}$Zn, $^{66}$Zn, and $^{68}$Zn with SM-3 $+0.392$, $+0.008$, and $+0.002$, and with SM-4 $+0.395$, $+0.112$, and $+0.003$, respectively. Both these calculations show a dramatic decrease in the $g(4_1^+)$ value for $^{68}$Zn, which is definitely closer to the observed behavior (see Fig. 5 and Table IV). As discussed in Ref. [3], this decrease is essentially due to the role played by the neutron $(0g_{9/2})^2$ admixture in the wave function of the $4_1^+$ state. Even if we change the single-particle energy spacing and get an improved $g(4_1^+)$ factor for $^{66}$Zn, both sets of calculations yield a significant decrease for $^{68}$Zn.

TABLE IV. Experimental $g$ factors in comparison to shell-model calculations SM-1 ($^{40}$Ca) and SM-2 ($^{56}$Ni, $g_{9/2}$) [1], SM-3 and SM-4 ($^{56}$Ni, $g_{9/2}$, see text and Refs. [2,3].)

| $^A$Zn Isotope | $g(2_1^+)$ | | | | | $g(4_1^+)$ | | | | |
|---|---|---|---|---|---|---|---|---|---|---|
| | Exp. | SM-1 | SM-2 | SM-3 | SM-4 | Exp. | SM-1 | SM-2 | SM-3 | SM-4 |
| $^{64}$Zn | $+0.45(3)$ | $+0.48$ | $+0.448$ | $+0.407$ | $+0.404$ | $+0.53(16)$ | $+0.730$ | $+0.362$ | $+0.392$ | $+0.395$ |
| $^{66}$Zn | $+0.45(3)$ | $+0.48$ | $+0.578$ | $+0.383$ | $+0.181$ | $+0.65(20)$ | $+0.740$ | $+0.436$ | $+0.008$ | $+0.112$ |
| $^{68}$Zn | $+0.50(3)$ | $+0.58$ | $+0.733$ | $+0.112$ | $+0.148$ | $-0.37(17)$ | $+1.08$ | $+0.404$ | $+0.002$ | $+0.003$ |

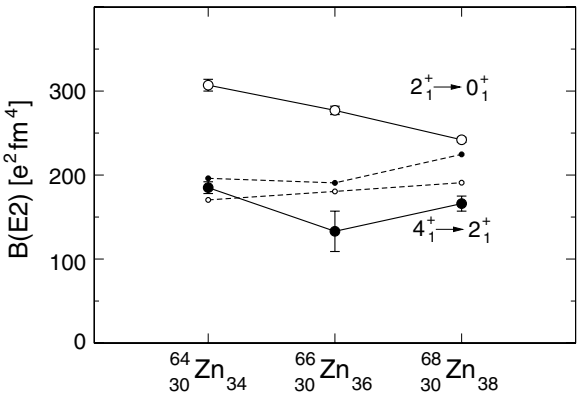


FIG. 6. $B(E2)$ values deduced from the measured lifetimes of the $2_1^+$ and $4_1^+$ states in $^{66}$Zn in comparison to corresponding results for the neighboring isotopes $^{64}$Zn and $^{68}$Zn [3]. Results from present large-scale shell-model calculations (SM-3) are also displayed (small symbols). The lines drawn are to guide the eye (see text).

## IV. SUMMARY AND CONCLUSIONS

The $g$ factor of the $4_1^+$ state in $^{66}$Zn has been measured for the first time. Its value, $g(4_1^+) = +0.65(20)$, agrees very well with that of its counterpart in the neighboring $^{64}$Zn, $g(4_1^+) = +0.53(16)$, but differs severely from the negative value, $g(4_1^+) = -0.37(17)$, of $^{68}$Zn. This result is incompatible with a transitional character that had been expected on the basis of calculations within the framework of the spherical shell model [3].

We also obtained a rather inaccurate value for the $3_1^-$ octupole state that is in fair agreement with the experimental values of corresponding states in $^{64}$Zn and $^{68}$Zn [2] and compatible with the collective value $g = Z/A = +0.45$.

In addition to the $g$ factors we have measured the lifetimes of several excited states in $^{66}$Zn via the DSAM technique. For the $2_1^+$ and $3_1^-$ states the literature values were confirmed. However, the lifetime of the $4_1^+$ state was found to be larger than the value obtained by Koizumi *et al.* [6] by a factor of 2. The lifetime of the $4_3^+$ state was determined for the first time.

All these new experimental data have been compared with corresponding values of neighboring $^{64}$Zn and $^{68}$Zn, and with results from new large-scale shell-model calculations. These calculations were based on $^{56}$Ni as a closed-shell core and the model space consisting of protons and neutrons occupying the $0f_{5/2}1p0g_{9/2}$ single-particle orbits. The results of these calculations provide clear evidence for the important role played by neutron $0g_{9/2}$ components in the nuclear wave functions. With these components in the wave functions the dependence of the $g(4_1^+)$ factor on neutron number and, in particular, its dramatic decrease from $^{64}$Zn to $^{68}$Zn is fairly well reproduced. In contrast, similar calculations with fitted interactions, such as those used in Ref. [1] or a recent fit to Ni, Zn, and Cu isotopes [16], give an overall more accurate spectroscopic description for these nuclei but tend to give a large and positive $g(4_1^+)$ factor for $^{68}$Zn in disagreement with the experimental value. An obvious improvement to all the latter calculations is to derive and use effective magnetic moments in the calculations of $g$ factors, as was done in Ref. [17].

In summary, the accumulated experimental information on $g$ factors and $B(E2)$ values for stable Zn isotopes calls for further theoretical examination.

## ACKNOWLEDGMENTS

The authors are grateful to the operating staff of the Munich tandem accelerator. Two of us, T.E. and M.H.J. are much indebted to Professors Alex Brown and Mihai Horoi for illuminating discussions. Support by the BMBF and the Deutsche Forschungsgemeinschaft is acknowledged.

[1] O. Kenn, K.-H. Speidel, R. Ernst, S. Schielke, S. Wagner, J. Gerber, P. Maier-Komor, and F. Nowacki, Phys. Rev. C **65**, 034308 (2002).
[2] J. Leske, K.-H. Speidel, S. Schielke, O. Kenn, D. Hohn, J. Gerber, and P. Maier-Komor, Phys. Rev. C **71**, 034303 (2005).
[3] J. Leske, K.-H. Speidel, S. Schielke, J. Gerber, P. Maier-Komor, T. Engeland, and M. Hjorth-Jensen, Phys. Rev. C **72**, 044301 (2005).
[4] F. Nowacki, Ph.D. thesis, IReS, Strasbourg, 1996.
[5] E. Caurier, F. Nowacki, A. Poves, and J. Retamosa, Phys. Rev. Lett. **77**, 1954 (1996).
[6] M. Koizumi *et al.*, Eur. Phys. J. A **18**, 87 (2003).
[7] J. Leske *et al.*, submitted to Phys. Rev. C.
[8] J. C. Wells and N. R. Johnson, program LINESHAPE, 1994, Oak Ridge National Laboratory (unpublished).
[9] F. J. Ziegler, J. Biersack, and U. Littmark, *The Stopping and Range of Ions in Solids* (Pergamon, Oxford, 1985), Vol. 1.
[10] K.-H. Speidel, O. Kenn, and F. Nowacki, Prog. Part. Nucl. Phys. **49**, 91 (2002).
[11] M. R. Bath, Nucl. Data Sheets **83**, 832 (1998).
[12] P. Raghavan, At. Data Nucl. Data Tables **42**, 189 (1989).
[13] R. Machleidt, Phys. Rev. C **63**, 024001 (2001).
[14] M. Hjorth-Jensen, T. T. S. Kuo, and E. Osnes, Phys. Rep. **261**, 125 (1995).
[15] H. Grawe, M. Gorska, M. Rejmund, M. Pfützner, M. Lipoglavsek, C. Fahlander, M. Hellström, D. Kast, A. Jungclaus, K. P. Lieb, R. Grzywacz, K. Rykaczewski, B. A. Brown, M. Hjorth-Jensen, and K. H. Maier, in *Highlights of Modern Nuclear Structure*, edited by A. Covello, (World Scientific, Singapore, 1999), p. 137.
[16] B. A. Brown, A. Lisetsky, and M. Horoi (unpublished).
[17] B. A. Brown, N. J. Stone, J. R. Stone, I. S. Towner, and M. Hjorth-Jensen, Phys. Rev. C **71**, 044317 (2005).